Coded Waveform Excitation for High-Resolution Ultrasonic Guided Wave Response

Mehmet K. Yücel, Sina Fateri, Mathew Legg, Adam Wilkinson, Vassilios Kappatos, Cem Selcuk, and Tat-Hean Gan

***Abstract*—Ultrasonic guided wave-based nondestructive testing systems are widely used in various fields of industry where the structural integrity of components is of vital importance. Signal interpretation in these systems might become challenging due to multimodal and dispersive response of the interrogated structure. These phenomena degrade the signal-to-noise ratio and also lower the spatial/temporal resolution. This paper compares the use of Maximal Length Sequences and linear chirp excitation signals to develop a novel signal processing technique using dispersion compensation and cross-correlation. The technique is applied to both simulated and experimental multimodal signals from an aluminium rod for performance assessment. It is quantitatively validated that the technique noticeably improves the signal-to-noise ratio of the guided wave response and is able to acquire an accurate time of flight of the individual wave modes, and hence, the propagation distance. The technique is compared for both linear chirp and maximal length sequences excitation signals. Noise analysis for these excitation signals is also presented.**

***Index Terms*—Broadband chirp, cross-correlation, dispersion compensation, maximal length sequences (MLSs), pulse compression (PuC), ultrasonic guided waves (UGWs).**

I. Introduction

OPERATIONAL and environmental factors affecting various components used in industry might eventually lead to degradation of the structural health of these components and could also raise health and safety concerns. Ultrasonic guided wave (UGW) testing, owing to its inherent long range coverage capabilities, emerged in the last decades as a popular nondestructive testing (NDT) technique to assess structural integrity of various components, generally for corrosion and flaws. In light of well-established theoretical advances and its swift adoption to industry, UGW has been popular for the inspection of structures such as pipes, plates, and rods, and more recently, for more complex structures such as cables and rails [1].

Manuscript received July 03, 2015; revised October 03, 2015 and October 25, 2015; accepted October 29, 2015. Date of publication November 18, 2015; date of current version February 02, 2016.

M. K. Yücel, M. Legg, V. Kappatos, C. Selcuk, and T.-H. Gan are with the Brunel Innovation Centre, Brunel University, Uxbridge, Middlesex UB8 3PH, U.K. (e-mail: mkerimyucel@gmail.com; bic@brunel.ac.uk).

S. Fateri is with Brunel University, Uxbridge, Middlesex UB8 3PH, U.K., and also with Plant Integrity Ltd., Granta Park, Great Abington, Cambridge CB21 6AL, U.K.

A. Wilkinson is with Plant Integrity Ltd., Granta Park, Great Abington, Cambridge, CB21 6AL, U.K.

Color versions of one or more of the figures in this paper are available online at http://ieeexplore.ieee.org.

Digital Object Identifier 10.1109/TII.2015.2501762

Although advances in hardware development and signal processing algorithms have paved the way for a better defect localization and characterization, various limitations still exist. Due to material and geometry dependent attenuation, inspection range is limited and less robust to noise. In addition to attenuation, several wave modes may exist depending on the material and geometry of the structure and the frequency contents of the wave. These wave modes generally experience dispersion, which leads to broadening of the pulses and thus degradation of the spatial resolution and localization of defects. In order to combat aforementioned problems, various signal processing algorithms have been proposed.

The autocorrelation properties of certain coded waveforms have been exploited for compressing the pulses. This technique, often referred to as pulse compression (PuC), has been adopted for applications such as material characterization [2]. In the NDT context, PuC is commonly used in air-coupled testing, since the high acoustic impedance mismatch between air and the transducers can lead to reduced signal-to-noise ratio (SNR) for this technique. Luo *et al.* used Golay codes to inspect aluminum plates [3], Senni *et al.* used chirp to inspect large forgings [4], and Zhang *et al.* used chirp signals to inspect steel pipes [5]. Other studies combined other techniques with PuC for further improvement; Zhou *et al.* combined wavelet transform and Barker codes to perform PuC [6] and Ricci *et al.* used chirp combined with ℓ^1-norm total variation deconvolution [7]. However, PuC performance is still limited in dispersive regions due to pulse broadening; hence there is a need for further advances to combat pulse broadening.

Dispersion compensation techniques, due to their capability of compressing (i.e., un-dispersing) dispersed signals, have been widely adopted for UGW-based NDT applications. Sicard *et al.* and Wilcox reported their pioneering methods to compensate for the effects of dispersion for UGW signals in [8] and [9]. Yamasaki *et al.* compared experimental and simulated time-reversed square pulses for dispersion compensation [10]. Even though SNR improvement is reported, no propagation distance-related information in a multimodal response are presented. Lin and Zeng proposed a chirp-based dispersion precompensation technique using *a priori* knowledge of propagation distance [11]. It is shown that the excitation signal can be tailored to achieve a good resolution to extract accurate time of flight (ToF). However, whenever multimodal responses are taken into account, the technique is not successful in extracting accurate ToF. Moreover, the technique is not automated, which makes it prone to human errors. Xu *et al.* used dispersion compensation in multimodal cases to estimate plate thickness, which can also

be used for propagation distance estimation [12]. Xu *et al.* also presented a wideband dispersion reversal (WDR) technique to self-compensate fundamental wave modes in a steel plate [13]. It is shown that the simulated WDR signals can effectively create single wave mode packets, which in turn identifies the modes effectively and also makes signal interpretation easier. However, WDR technique requires *a priori* knowledge on the propagation distance in this paper, though it has the potential to work without the need of propagation distance, as it is capable of thickness evaluation [14]. Several studies have combined PuC with dispersion compensation for further SNR and localization improvement. Toiyama and Hayashi used PuC with dispersion compensation using chirp waveforms [15]. However, no quantitative SNR improvement was presented in this paper and the technique was applied to single wave mode scenarios. Marchi *et al.* used PuC with warped frequency transform (WFT)-based dispersion compensation technique to enhance the localization of a steel cylindrical mass (a simulated defect) in an aluminium square plate [16]. However, the technique requires wavelength filtering to effectively reduce the effect of multimodal propagation. In one of the latest studies, Marchi *et al.* extended WFT-based dispersion compensation to irregular wave guides and combined it with PuC [17]. However, no experimental validation was presented and triangular pulse excitation was used.

This paper utilizes Maximal Length Sequence (MLS) signals to produce a brute-force search-based automated technique using dispersion compensation and cross-correlation to locate defects. The short-time Fourier transform (STFT) is used to obtain spectrograms for time-frequency visualization of the signal. This is one of several time–frequency representations (TFR), such as Wigner–Ville [18], which could have been used. The performance of the technique using MLS is assessed and compared with a linear broadband chirp. It is shown that such a combination with cross-correlation can improve SNR and facilitate the accurate extraction of ToF, thus the propagation distance, even in complex multimodal scenarios.

This paper is organized as follows. The theoretical background is given in Section II and the proposed technique is described in Section III. First, the technique is applied to synthesized MLS and chirp waveforms in Section IV and then to experimentally acquired MLS and chirp waveforms in Section V. The noise performance of the technique is also presented in Section V.

II. Theoretical Background

A. Pulse Compression

PuC techniques have been developed for applications such as electromagnetic (EM) radar systems, to strike a balance between detection of close reflectors, coverage range, and hardware output power; and also to acquire the impulse response of a system [19]. For the proper exploitation of the technique, a signal with a good autocorrelation function $\mathrm{ccf}(x(t), x(t)) \cong \delta(t)$ is required. Signals with satisfactory autocorrelation properties that have been commonly used are chirped sinusoids or pseudorandom binary sequences. Barker codes, MLS, Gold codes, Golay codes, Chaos sequence, and Legendre sequence are examples of pseudorandom binary sequences used in [20]. In this paper, MLS and linear chirp signals are used and thus explained in the following parts.

B. Maximal Length Sequences

MLS are generated using linear feedback shift registers (LFSRs) with N-delay taps, resulting in a sequence of length $L = 2^N - 1$. The autocorrelation function of a L-length MLS, an important feature exploited in this paper, is given as

$$\mathrm{ccf}_{a,a}(t) = \begin{cases} 1, & \text{lag} = 0 \\ 1/L, & \text{lag} \neq 0. \end{cases} \tag{1}$$

It has a δ-function like autocorrelation function and has a flat spectral density with a near-zero dc component. More information about MLS can be found in [21].

C. Chirp

Chirped sinusoids are broadband signals, which can be created and tailored according to the frequency components desired in the signal. Chirp signals might have positive or negative chirp rates, i.e., the instantaneous frequency increases or decreases with time, and moreover, it could have linear or nonlinear trajectories. Since linear chirp signals are used in this study, a generic linear chirp equation is given as

$$x(t) = \sin\left(\theta_0 + 2\pi \left[f_0 + \frac{a}{2}\, t\right] t\right) \tag{2}$$

where θ_0 is the initial phase, f_0 is the starting frequency, and a is the chirp rate, which is given as

$$a = \frac{f_1 - f_0}{t_1} \tag{3}$$

where f_1 is the final frequency of the chirp and t_1 is the corresponding time of the final frequency. The instantaneous frequency $f(t)$ may be calculated from the rate of change of the phase of (2) giving

$$f(t) = \frac{1}{2\pi}\frac{\partial}{\partial t}\left(\theta_0 + 2\pi \left[f_0\, t + \frac{a}{2}\, t^2\right]\right) = f_0 + a\, t. \tag{4}$$

D. Dispersion Compensation

Dispersive wave modes spread out over time and space during propagation, which lowers the spatial resolution and complicates the signal interpretation accordingly. Dispersion compensation techniques [8], [9] have been used to un-disperse the dispersed signals to combat spatial resolution degradation. The algorithm used in this paper is originally published in [9], and it makes use of *a priori* knowledge of the dispersion curve of a UGW mode and maps signals from time domain to spatial domain and thus reverses the dispersion process.

It is assumed that the transducer is ideal and only excites the desired wave modes at the given location. The received signal $\tilde{x}(t)$ at a given propagation distance d may be modelled [9] as

$$\tilde{x}(t) = \sum_j \int_{-\infty}^{+\infty} A_j(\omega)\, F(\omega)\, e^{i\,(-k(\omega)\,d + \omega\, t)}\, d\omega \tag{5}$$

where $A_j(\omega)$ is the reflection coefficient of each reflector (assumed frequency independent and constant throughout this paper), $F(\omega)$ is the Fourier transform of the input signal $f(t)$ excited at $d = 0$, ω is the angular frequency, and $k(\omega)$ is the wavenumber defined as

$$k(\omega) = \frac{\omega}{V_{\text{ph}}} \tag{6}$$

where V_{ph} is the phase velocity of the wave. The effect of dispersion can be eliminated by choosing a centre frequency for dispersion compensation f_c and then adjusting the other frequency components to centralize all frequency components at time $\tau = d/V_{\text{gr}}(f_c)$, where V_{gr} is the group velocity of the wave. Waveform $h(t)$, which is dispersion compensated for distance d, can then be written as

$$h(t) = \int_{-\infty}^{+\infty} G(\omega)\, e^{i\,(k(\omega)\,d + \omega\,(t-\tau))}\, d\omega \tag{7}$$

where $G(\omega)$ is the Fourier transform of the received signal $\tilde{x}(t)$. Once the compensated signal is acquired, the acquired time trace can be converted to distance domain using

$$d = V_{\text{gr}}(f_c)\, t \tag{8}$$

where $V_{\text{gr}}(f_c)$ is the group velocity for a single central frequency f_c. In this work, this f_c was chosen to be the frequency component of the signal with highest amplitude, which was the technique used by Wilcox [9]. While this is an obvious choice for narrow band signals, it is less so for broadband signals and can potentially be a source of error.

III. Proposed Technique

A dispersed signal can be compensated for the degrading effects of dispersion using (7). Although it would have better SNR and localization compared to its raw version, in more complex scenarios, signal interpretation could still be difficult. In such cases, PuC technique can be used to further improve SNR and localization.

A dispersion compensated signal, denoted by $\tilde{x}(t)$, would have good cross-correlation with $x(t)$; the signal excited from the transducer. Maximum value of their cross-correlation $\max(\text{ccf}(\tilde{x}(t), x(t)))$ would provide the accurate location of the defect echo.

A technique is presented in this paper, which combines PuC with dispersion compensation in an iterative manner. The dispersed signal $\tilde{x}(t)$ is compensated for the dispersion that a single wave mode would experience for a propagation distance $d(n)$. This dispersion compensated version of the received signal $h_{d(n)}(t)$ is then cross-correlated with the excitation signal. The maximum value $c_{d(n)}$ of the cross-correlation output is obtained. This process is repeated for a range of propagation distances $d = [d(1), \ldots, d(n), \ldots, d(N)]$. The output of this iterative process is an array of maximum cross-correlation values $c = [c_{d(1)}, \ldots, c_{d(n)}, \ldots, c_{d(N)}]$, where each value corresponds to a different propagation distance. Echoes from defects ideally should show up as peaks in these maximum cross-correlation values. Such an iterative analysis would also remove the need for *a priori* knowledge on the propagation distance for accurate dispersion compensation. It must be noted that although the dispersion compensation is performed for a single wave mode, propagation distance would still be extracted successfully for multimodal cases. This is due to the fact that the other wave mode (not dispersion compensated) would either be under compensated or over compensated, since the existing wave modes are unlikely to have the exact dispersion curve. This under compensation or over compensation would lead to degraded results for that specific propagation distance (which is not the correct propagation distance), thus eliminating the need for multiple mode compensation at the same time.

A. Noise Performance Analysis of the Proposed Technique

The effect of noise on the proposed technique for experimental signals were analyzed using the introduction of additive white Gaussian noise (AWGN) of different levels (-20 to 20 dB, with 5 dB steps). SNR values throughout the paper were calculated as follows:

$$\text{SNR} = 20\ \log_{10}\left(\frac{|P_e|}{\sigma_{x(t)}}\right) \tag{9}$$

where P_e is the echo's peak amplitude and σ is the standard deviation of $x(t)$, the signal under consideration [22]. The noise addition procedure has been repeated 100 times for each noise level and proposed technique is then applied on noisy signals. In the noise-analysis section, which is performed only for experimental signals, only flexural-based compensation is considered. Extracted propagation distance values are divided into four categories and defined as follows.

Let d be the extracted propagation distance with additive noise for chirp and MLS and d_x be the extracted propagation distances to be used as references (without the added noise) for chirp and MLS. The noisy signal classification is then performed using four classes: 1) class 1 ($d = d_x \pm 0.05$ m); 2) class 2 ($d = d_x \pm 0.5$ m); 3) class 3 ($d = d_x \pm 1$ m); and 4) class 4 ($d < d_x - 1$ m or $d > d_x + 1$ m). Results of this noisy signal detection classification are presented in Tables III and IV.

IV. Signal Synthesis

The proposed technique was first analyzed with simulated signals using chirp and MLS excitation signals. The chirp signal (500 samples) was created using (2) with $f_o = 10$ kHz, $f_1 = 125$ kHz, and $t_1 = 0.5$ ms, and a sampling rate of 1 MHz. The MLS excitation signal (127 samples) was sampled at 250 kHz, which results in a signal that has time-invariant broadband frequency components up to 125 kHz (Nyquist rate).

Dispersion simulations were performed for an aluminium cylindrical solid rod with a diameter of 8 mm for the fundamental flexural and longitudinal wave modes. Group velocity dispersion curves for this rod were obtained using Disperse,[1] see Fig. 1. The excitation signals were artificially dispersed

[1] [Online]. Available: http://www3.imperial.ac.uk/nde/products.

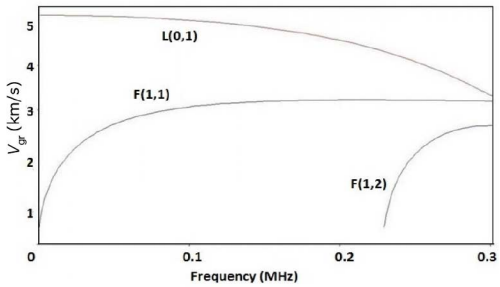

Fig. 1. Group velocity (V_{gr}) dispersion curves of an aluminium rod of 8 mm diameter. All existing modes (except fundamental torsional mode) up to 300 kHz are shown and indicated in the plot.

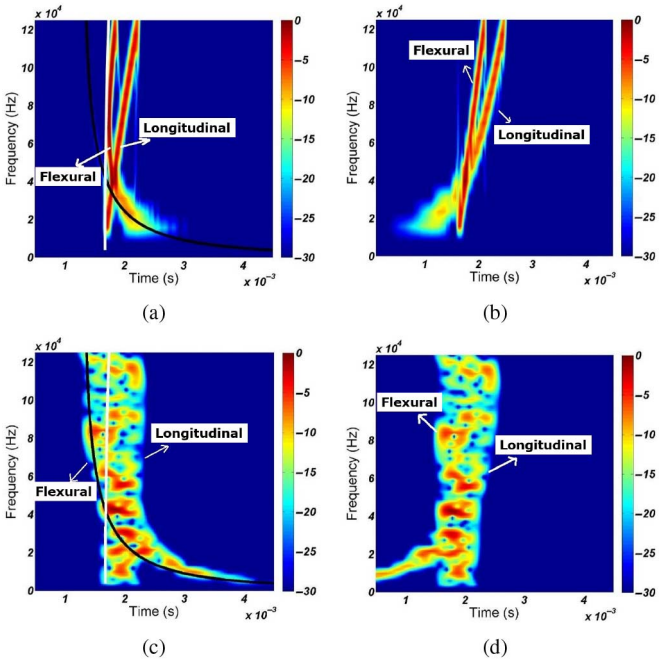

Fig. 2. STFT representations of simulated multimodal signals for (a) linear chirp and (c) MLS. The theoretical arrival times are overlaid for the fundamental flexural (black solid lines) and longitudinal (white solid lines) wave modes. Propagation distances for these two wave modes were 4.3 and 8.6 m, respectively. The dispersion compensated versions of the signals are plotted for (b) chirp and (d) MLS, where the compensation is performed for the flexural wave mode and for a propagation distance of 4.3 m. The center frequency for dispersion compensation was 48 kHz.

for the flexural wave mode, assuming a propagation distance of 4.3 m (first echo from the end of the rod). The same process was performed for the longitudinal wave mode, assuming a propagation distance of 8.6 m (second echo). These two dispersed signal were then summed. It can be seen that this case results in these two wave modes being superposed, as opposed to simpler cases such as two wave modes being dispersed for the same propagation distance, where two reflections will not be superposed. Mode and frequency dependent attenuation was ignored.

A. Flexural Mode Compensation

Dispersion compensation was first performed on the flexural wave mode, assuming a propagation distance of 4.3 m. Fig. 2(a)

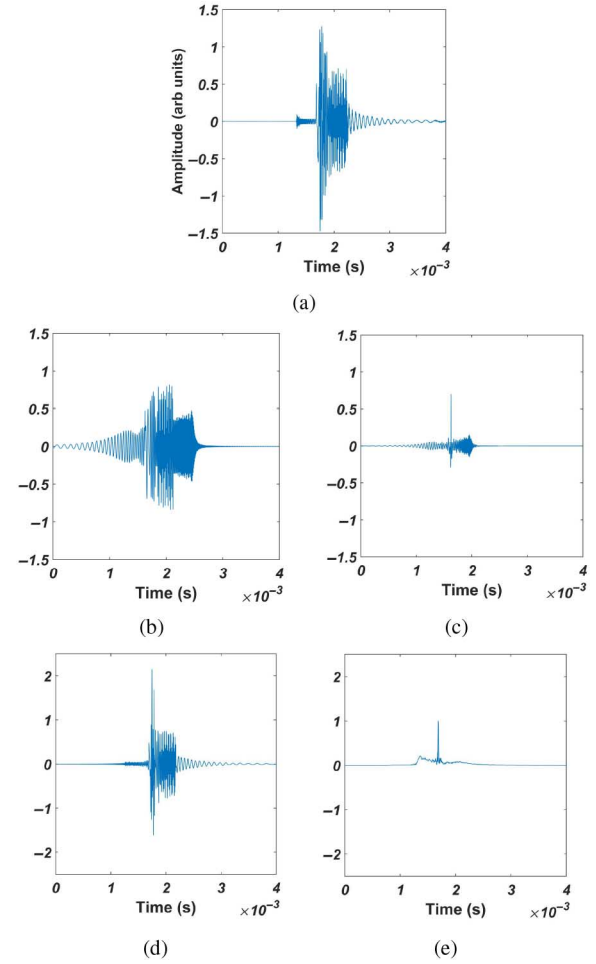

Fig. 3. Plots show the windowed time-domain representations of simulated (a) chirp signal, (b) dispersion-compensated chirp signal, where the compensation has been performed for the flexural wave mode echo, which has propagated a distance of 4.3 m, and (c) cross-correlation between excitation and dispersion compensated chirp signal. The corresponding dispersion compensated and cross-correlatated signals for the longitudinal mode echoes are shown in (d) and (e).

and (c) shows the STFT representations of dispersed signals for chirp and MLS excitations, respectively. Plots shown in Fig. 2(b) and (d) shows the dispersion compensated (for 4.3 m) time traces for chirp and MLS excitations. It is evident that the first wave packets (the flexural wave mode) are compensated for dispersion (since they are the same with the transmit signal spectrogram), whereas the second wave packets (the longitudinal wave modes) are further dispersed, since two wave modes have different dispersion curves. Fig. 3 (a)–(c) shows time domain plots of the dispersed signal, compensated signal (for the flexural wave mode and the correct propagation distance) and the cross-correlation of the excitation and compensated signals for chirp excitation. Refer to [23] for corresponding plots for MLS excitation. As can be seen in previously mentioned figure, multimodal time traces are successfully compressed.

The iterative search technique was applied on the above-mentioned signals for a range of distances between 0 and 10 m with a step size of 1 cm. Although the interference of the longitudinal wave mode resulted in higher cross-correlation values for incorrect distances, the iterative technique still managed to

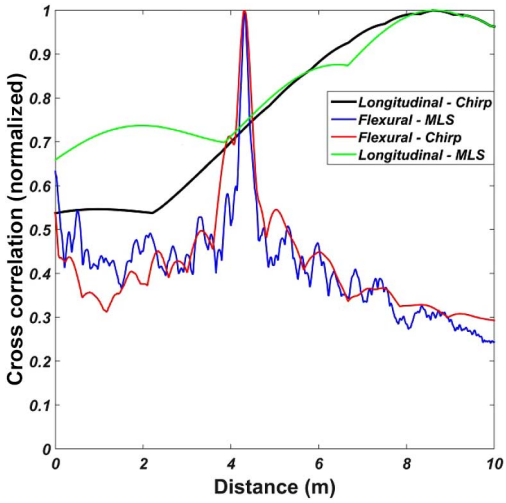

Fig. 4. Plot shows the results of the iterative technique for the signal synthesis; maximum cross-correlation trace, as a function of distance, of chirp (red) and MLS (blue) signals (compensation performed on flexural). Longitudinal-based compensation results are shown in black and green lines (chirp and MLS). All cases managed to extract the exact propagation distance. Results are obtained by applying the iterative technique with 0.01-m distance resolution.

TABLE I
SIMULATION SNR VALUES FOR CHIRP AND MLS EXCITATION SIGNALS. "RAW" COLUMNS ARE THE SNR VALUES OF RAW SIGNALS, THE "RESULT" COLUMNS ARE RESULTING SNRS OF DISPERSION COMPENSATED AND THEN COMPRESSED PULSES

Signal	Mode	Raw (dB)	Result (dB)	Increase (dB)
Chirp	Longitudinal	25.091	32.4009	7.3099
	Flexural	25.9025	37.6422	11.7395
MLS	Longitudinal	23.9557	30.3264	6.3707
	Flexural	21.9279	32.9654	11.0375

extract the exact propagation distances both for chirp and MLS signals. Results are shown in Fig. 4.

Quantification of the SNR improvement for signals can be seen in Table I. The SNR improvement for the MLS signal is approximately the same as the chirp's SNR improvement (which are 11 and 11.7 dB, respectively). Chirp is fairly self compensated for dispersion and it has a higher peak in the first wave packet (which corresponds to flexural wave mode).

SNR improvements for both signals are approximately the same and satisfactory.

B. Longitudinal Mode Compensation

The simulation of dispersion compensation and cross-correlation was implemented with compensation for the longitudinal wave mode and an assumed propagation distance of 8.6 m. Other parameters and signals were the same as for Section IV-A. Fig. 3(a) shows the simulated dispersed signals for chirp. The dispersion compensated signal for the longitudinal mode and cross-correlation are shown in Fig. 3(d) and (e). Refer to [23] for corresponding plots for MLS. It can be seen that the compensated signals are similar to dispersed signals. This can be explained by the fact that longitudinal wave mode is not dispersed much, even for a propagation distance of

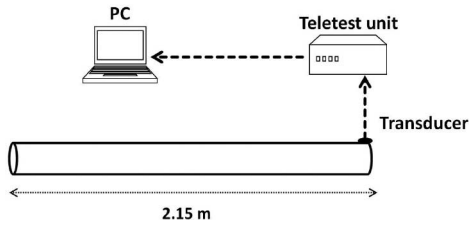

Fig. 5. Representative diagram for the experimental setup.

8.6 m. The compensated chirp shows a relatively distinct peak compared to compensated MLS, which is nearly the same as its raw (dispersed) version. Following the dispersion compensation, when signals are compressed, distinct peaks are observed for both chirp and MLS signals. In addition to the localization-wise improvement, SNR improvements are also clear for both signals. Approximately 7 and 6 dB increase in SNR values are observed for chirp and MLS, respectively. These results follow the trend seen in Section IV-A, where SNR improvements for both signals are similar.

The iterative search technique is applied on the above-mentioned signals for a range of distances between 0 and 10 m with a step size of 1 cm. Extracted propagation distances for longitudinal-based compensation are expected to be worse than flexural-based compensation due to the former's nondispersive nature (which leads to high cross-correlation values for all distances the technique is applied for), yet MLS and the chirp signal managed to extract the exact propagation distances. Results are shown in Fig. 4.

V. EXPERIMENTATION

A. Experimental Setup

The iterative technique is assessed through experimentation on a 2.15-m long aluminium cylindrical rod of 8 mm diameter (same structure that is modelled in Section IV). The same dispersion curves shown in Fig. 1 are used in this section.

A single shear-mode lead zirconium titanate (PZT) transducer was attached to one end of the rod with a clamp (configured to exert uniform force on the transducer) in pulse echo configuration. These transducers have been reported to have a sufficiently flat frequency response in the desired frequency spectrum [24]. A Teletest[2] unit was used to drive the transducer. The analogue input sampling rate was set to 1 MHz. Power gain levels were fixed to 10 dB. No averaging was performed on received signals. The received signals were then transferred to a PC for analysis in MATLAB. A representative diagram of the experimental setup is shown in Fig. 5.

The signals (both received and excited), before being fed to the iterative technique, were normalized via ℓ^2-normalization to make sure both signals are comparable in terms of power. The excitation signals were a 250-sample positive linear chirp sampled at 1 MHz that has frequency components between 10 and 125 kHz and a 63-sample MLS sampled at 250 kHz. The durations of the MLS and chirp excitation signals were thus approximately the same (0.26 and 0.25 ms, respectively). The

[2][Online]. Available: http://www.teletestfocus.com/teletest-focus-plus/.

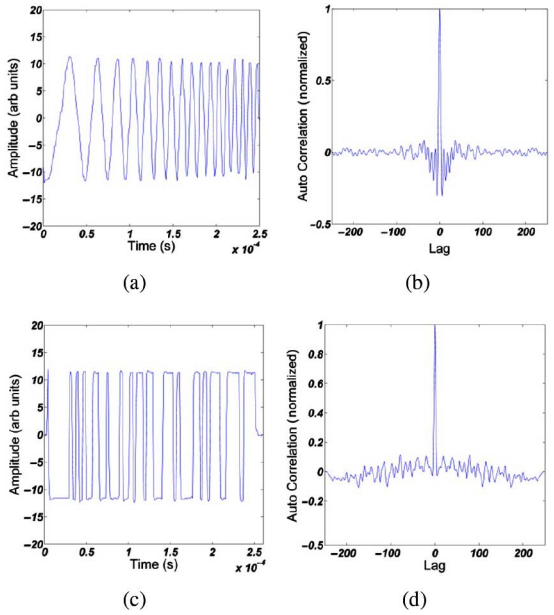

Fig. 6. Chirp excitation signal and its auto correlation are shown in plots (a) and (b), respectively. The corresponding plots for MLS are shown in (c) and (d), respectively.

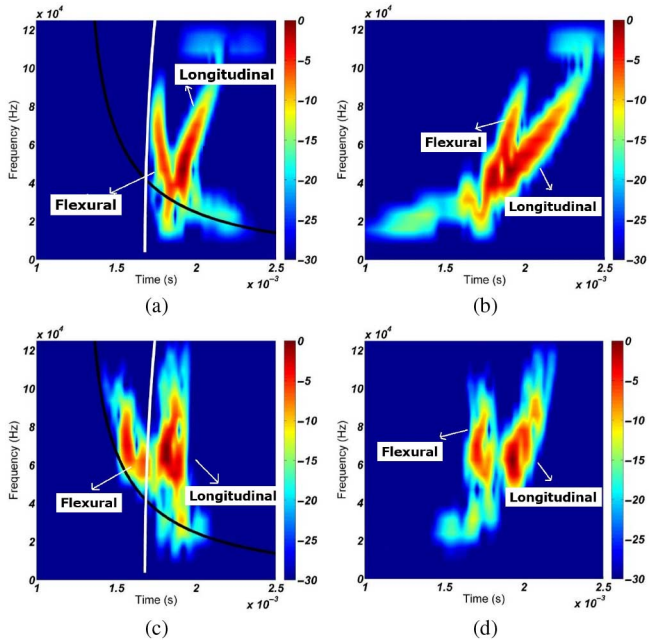

Fig. 7. Time windowed measured signals' spectrograms with fundamental flexural (black solid lines) and longitudinal (white solid lines) V_{gr} dispersion curve overlaid. Shown plots are (a) linear chirp, (b) dispersion compensated linear chirp, (c) MLS, and (d) dispersion compensated MLS. Two wave modes shown in (a) and (c) are the first echo of the fundamental flexural mode and the second echo of the fundamental longitudinal mode. Dispersion compensation is based on the flexural wave mode and it is performed for a propagation distance of 4.3 m. Center frequency for dispersion compensation is 48 kHz.

excitation signals can be affected by the transfer function of the hardware and the transducers. As this has the potential to influence the effectiveness of the cross-correlation technique, the output signal generated by the Teletest unit, with a transducer as a load, was measured using an oscilloscope, see Fig. 6(a) and (c). These signals were used in this work with experimental data for obtaining propagation distances.

B. Experimental Results

The received signals are windowed to obtain a certain part of the signal that contains only two echoes (first echo of flexural and second echo of longitudinal), see Fig. 7(a) and (c). It must be noted that the wave modes arising from the chirp and MLS excitation are superposed in the frequency region of 20–65 kHz and 20–80 kHz, respectively [Figs. 7(a) and (c)]. The transmit waveforms for both chirp and MLS had been designed to have frequency components up to 125 kHz. Therefore, the received signals were filtered to remove the frequency components beyond the frequency region of interest. This was achieved using a square low-pass window function. Due to the coupling of the transducer, the fundamental torsional wave mode is not excited. Equation (8) was used to convert the time trace to distance using a central frequency f_c of 48 kHz. This corresponds to the highest amplitude frequency component in the signal.

C. Flexural Mode Compensation

The dispersed, compensated (for the flexural wave mode and a propagation distance of 4.3 m), and compressed signals are shown in Fig. 8 for the chirp signal. Readers are referred to [23] for the corresponding plots of MLS. The chirp signal exhibits a temporally spread behavior and the wave modes can not be distinguished from each other. After the dispersion compensation and cross-correlation, as shown in Fig. 8(b) and (c), chirp signal has a clearly better SNR value based on the flexural wave mode. Sharp peaks also show a pronounced improvement in localization of structural discontinuities. The SNR improvement for MLS and chirp are reported as 4.8 and 11 dB, respectively. SNR improvement for the experimental signals are also shown in Table II.

The iterative search for the cross-correlation maximum is performed for ranges between 0 and 10 m with a step size of 0.01 m. The multimodal nature of the signals (especially the longitudinal wave mode as it has low dispersion) and the effects of hardware/transducer imperfections lead to high cross-correlation values in short distances, as shown in Fig. 9. To overcome this, one can look at the maximum cross-correlation of the wave mode of interest rather than the entire signal. This, however, would require accurate spatial/temporal separation of two modes, which may not be feasible in scenarios where modes are heavily superposed. A simple peak detection algorithm based on the prominence characteristics of the peaks is derived to address this issue. As observed in Fig. 9, peak values that have a rather uniform drop off on both sides of the peaks indicate the actual propagation distance. Therefore, to distinguish actual peaks from the oscillatory peaks in the first 1 m, above-mentioned characteristics of the actual peaks is exploited, and accurate results are obtained; 4.29 m for MLS and 4.39 m for chirp, which yields 0.01 m error for MLS and 0.09 m error for chirp. It must also be noted that results are within 0.01-m confidence level due to step size of distance (0.01 m).

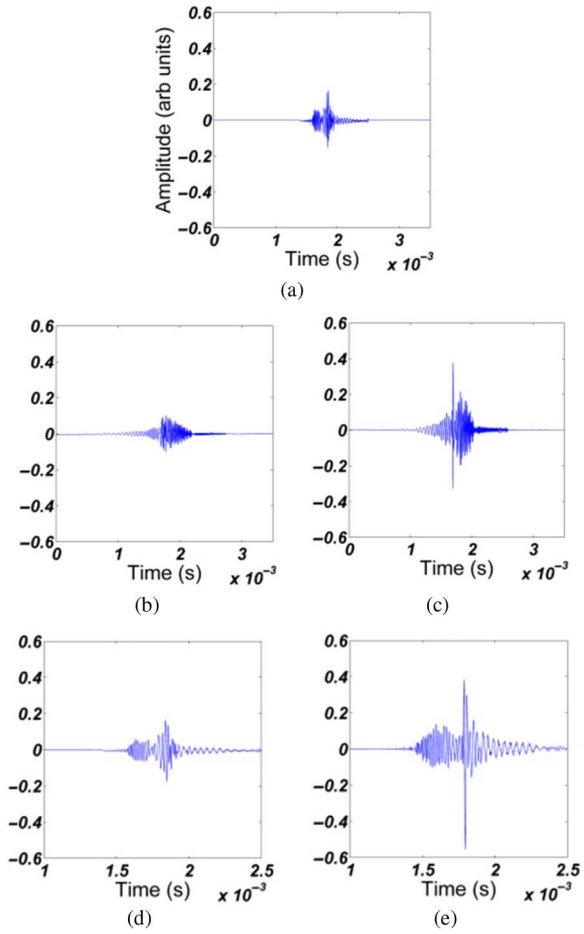

Fig. 8. Example plots show the windowed time domain representations of (a) measured chirp signal, (b) dispersion compensated chirp signal, where the compensation has been performed for the flexural wave mode echo which has propagated a distance of 4.3 m, and (c) cross-correlation between excitation and dispersion compensated chirp signal. Plot (d)–(e) shows the corresponding signals for the longitudinal dispersion compensation.

TABLE II
SNR VALUES FOR CHIRP AND MLS EXCITATION SIGNALS. "RAW" COLUMNS ARE THE SNR VALUES OF RAW SIGNALS, THE "RESULT" COLUMNS ARE RESULTING SNRS OF DISPERSION COMPENSATED AND THEN COMPRESSED PULSES

Signal	Mode	Raw (dB)	Result (dB)	Increase (dB)
Chirp	Longitudinal	19.0	26.6	7.6
	Flexural	13.3	24.4	11.1
MLS	Longitudinal	22.5	28.0	5.5
	Flexural	18.6	23.4	4.8

D. Longitudinal Mode Compensation

The iterative technique is also implemented for dispersion compensation of the longitudinal mode and a propagation distance of 8.6 m. Examples of the dispersed, longitudinal mode dispersion compensated, and the cross-correlation of the transmit and dispersion compensated signal can be seen in Fig. 8 (a), (d), and (e), respectively. Refer to [23] for corresponding plots for MLS. It can be seen that the dispersed raw signal is approximately the same with the longitudinal dispersion compensated signal since the longitudinal mode experiences low dispersion.

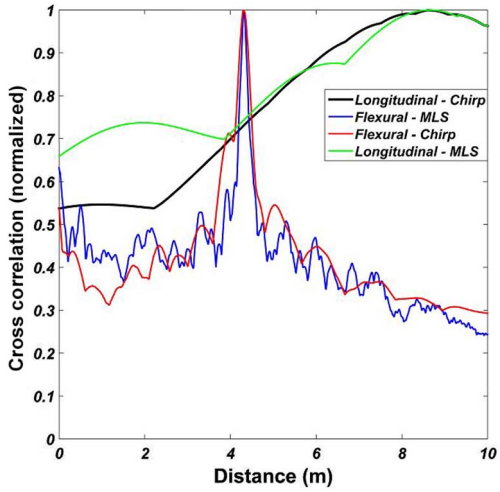

Fig. 9. Plot shows the results of the iterative technique for the windowed data; maximum cross-correlation trace, as a function of distance, of chirp (red) and MLS (blue) signals (compensation performed on flexural). Longitudinal-based compensation results are shown in black and green lines (chirp and MLS). The iterative technique failed to extract the correct propagation distance (8.6 m for longitudinal) in the case of longitudinal compensation. Results are obtained by applying the iterative technique with 0.01-m distance resolution.

After dispersion compensation and PuC, both chirp and MLS show distinct peaks for the second wave packet (the longitudinal mode). SNR values for this section can be found in Table II.

Similar to previous results, MLS had a lower SNR improvement compared to chirp (5.5 and 7.5 dB, respectively). The SNR improvement for MLS for flexural and longitudinal modes are close. However, the SNR improvement for chirp for flexural and longitudinal modes are not that similar. It can, therefore, be said that the iterative technique based on longitudinal-based compensation offers a good SNR improvement for both signals, albeit slightly worse than flexural-based compensation.

The iterative technique had worked well for the flexural mode in terms of detecting the location of defects. However, it did not perform well in extracting the propagation distance for the longitudinal mode for MLS and chirp signals used. The traces shown in Fig. 9 have low variance and the peaks of these traces are different from the expected value of 8.6 m. The rather low variance of the traces is due to the inherent minimal dispersion that the longitudinal mode undergoes. Although the peak values of the longitudinal-based compensation trace should give close values to the correct propagation distance nonetheless (as observed in the longitudinal-based simulation section), the sensitivity to the noise as well as the frequency response of the medium indicate the iterative technique fails to extract the correct propagation distance for longitudinal-based compensation.

E. Noise Performance

Detection performance of chirp and MLS vary under different noise levels. As expected, in high-noise levels such as -20 dB, the percentage of the accurate results (Class 1 in Tables III and IV) obtained is really low. As the noise power decreases, number of accurate detections both for chirp and

TABLE III
DETECTION RATES (OUT OF 100 REPETITIONS) OF THE TECHNIQUE (FOR FLEXURAL MODE COMPENSATION) USING EXPERIMENTAL SIGNALS WITH VARIOUS NOISE LEVELS (−20 TO 20 dB) FOR MLS EXCITATION. EACH COLUMN REPRESENTS A NOISE POWER AND EACH ROW REPRESENTS A DIFFERENT CLASSIFICATION. CLASS DEFINITIONS ARE EXPLAINED IN IN SECTION III-A

Class	−20	−15	−10	−5	0	5	10	15	20
1	1	7	5	12	30	36	58	87	94
2	17	17	27	33	47	48	64	87	94
3	28	31	29	33	47	48	64	87	94
4	72	69	71	67	53	52	36	13	6

TABLE IV
DETECTION RATES (OUT OF 100 REPETITIONS) OF THE TECHNIQUE (FOR FLEXURAL MODE COMPENSATION) USING EXPERIMENTAL SIGNALS WITH VARIOUS NOISE LEVELS (−20 TO 20 dB) FOR CHIRP EXCITATION. EACH COLUMN REPRESENTS A NOISE POWER AND EACH ROW REPRESENTS A DIFFERENT CLASSIFICATION. CLASS DEFINITIONS ARE EXPLAINED IN SECTION III-A

Class	−20	−15	−10	−5	0	5	10	15	20
1	2	11	22	41	52	59	61	83	89
2	13	28	49	75	89	99	100	100	100
3	24	36	49	75	89	99	100	100	100
4	76	74	51	25	11	0	0	0	0

MLS excitations increase. However, as can be seen in Tables III and IV, chirp excitation has a better performance in terms of number of accurate detections as the noise power decreases. Under 0 dB noise, for instance, chirp has 52% accurate detection rate whereas MLS excitation has only 30%. However, both MLS and chirp excitations have around 90% accurate detection rates as the noise power is lowered to 20 dB, which makes them feasible for this technique. It must be also noted that, as explained in the noisy signal classification, extracted propagation distance for the chirp signal is already 0.08 m off than MLS.

In this work, the excitation duration, time bandwidth (TB), was relatively short. The experimental excitation durations were about half that of the simulated signals. This may have had an effect on the noise performance of the cross-correlation technique and may have introduced some mathematical noise, such as an increase in cross-correlation sidelobes. It is possible that this may have had a more detrimental effect for MLS excitation than chirp in the presence of additive noise. In the future work, excitation signals with different TBs should be investigated to see what effect this has on the achieved accuracy.

F. Remarks and Recommendations

Fig. 9 showed that the flexural-based compensation had minor errors whereas longitudinal-based compensation had large errors. It must be emphasized that the frequency characteristics of the transducers and the hardware are influential factors for the iterative technique. The results indicate that this technique is more suited for dispersive wave modes. Although simulation results provided accurate propagation distances, arbitrary noise coupled with hardware/sensor imperfections are likely to have led to the above-mentioned errors in experimental results.

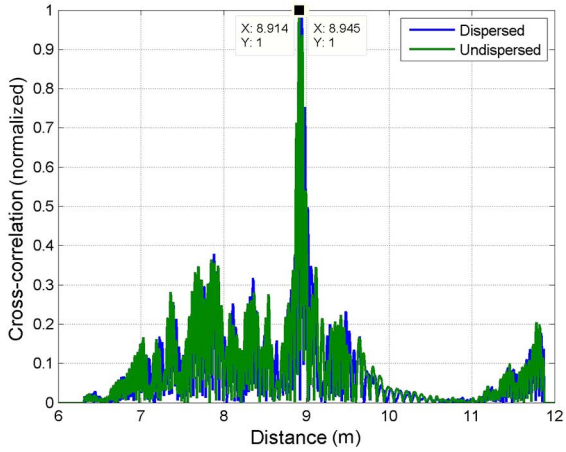

Fig. 10. Plot showing cross-correlation of dispersed and undispersed signals, where dispersion compensation was performed for the longitudinal wave mode for chirp excitation.

The technique was also implemented with a lower distance increment (0.0001 m). It was observed that the technique produced the same peak values at close distances, which means multiple maximum propagation distances were extracted. This could be caused by the available resolution of the V_{gr} dispersion curve data used for compensation. As the V_{gr} dispersion curve data had to be interpolated to cover a wide frequency range for compensation, it is likely that this interpolation caused minor errors in certain frequencies V_{gr} values. Although not visible up to certain distance increment, it was visible in (0.1 mm) distance increment resolution. Therefore, the relatively low resolution of V_{gr} data can effectively be the reason of failed propagation distance extraction for longitudinal mode presented in Section V, since this mode goes through minimal dispersion which might not be resolved properly by the available V_{gr} data.

VI. COMPARISON WITH CROSS-CORRELATION OF DISPERSED AND UNDISPERSED SIGNALS

The longitudinal mode, in the frequency range of interest, has relatively low dispersion. It, therefore, might be expected that cross-correlation of the transmit signal with the dispersed signal might be able to be used for distance estimation without the use of dispersion compensation. Therefore, a comparison was made of the propagation distances obtained using cross-correlation of the transmit signal with both the dispersed signal and dispersion compensated signals, where compensation was performed for the longitudinal wave mode. The dispersion compensation was performed for the entire time trace, refer to reference [25] for more detail. The resulting cross-correlated signals can be seen in Fig. 10. The differences between the cross-correlated peak times for dispersed and dispersion compensated signals were small. These peak times were converted into propagation distances using (8) and a group velocity of 5094 m/s, which corresponded to a central frequency f_c of 48 kHz. For chirp excitation, distances of 8.93 and 8.91 m were obtained for, respectively, dispersed and dispersion compensated signals. The corresponding distances for MLS excitation were 8.95 and

8.91 m. These are higher than the actual propagation distances of 8.6 m (four lengths of the rod). This error could be related to the group velocity used, though more investigation is required. This noniterative technique was tried for the dispersive flexural wave mode but struggled to achieve accurate results.

VII. Conclusion

A novel iterative technique combining brute-force search-based dispersion compensation and PuC was presented using broadband MLS excitation. The technique iteratively searches for the correct propagation distance using *a priori* knowledge of the group velocity dispersion curve. Following a thorough signal modelling and comparison between MLS and linear broadband chirp waveforms, experimental performance of MLS was assessed and compared with linear broadband chirp. Measurements were made on a 2.15-m long solid aluminium rod using pulse echo configuration. It is observed that despite the heavily superposed wave modes and measurement noise, the iterative technique extracted an accurate propagation distance for MLS with 1 cm error, which was superior to chirp with 9 cm error, for the highly dispersive flexural wave mode.

A significant SNR improvement, slightly better for chirp compared to MLS, was achieved for both excitation waveforms (Table II). The iterative technique was assessed for SNR improvement and propagation distance extraction using various wave modes both experimentally and through signal synthesis (dispersive fundamental flexural and nondispersive fundamental longitudinal). Experimental results indicate that although SNR improvement can be achieved both for dispersive or nondispersive wave modes, the propagation distance extraction is successful only for dispersive wave modes. Noise analysis conducted for the dispersive wave mode shows that linear broadband chirp signal performs better than MLS in terms of accurate extraction of propagation distance.

The iterative technique had worked well for the highly dispersive flexural wave mode, but had not worked for the relatively nondispersive longitudinal wave mode. Cross-correlation was, therefore, also performed using a single cross-correlation of the transmit signal with both dispersed and dispersion compensated signals, where compensation was performed for the longitudinal mode. The propagation distances obtained were relatively similar for both dispersed and undispersed signals for chirp and MLS. However, an overestimation in the propagation distance of about 8–9 cm was obtained.

Overall, the findings of this paper indicate that the iterative technique was successful for dispersive wave modes for MLS and chirp excitation waveforms. However, for wave modes which experience little dispersion, it was found that cross correlation of the transmit and received signals was more suited and that dispersion compensation may not increase the accuracy significantly. While these techniques have been used for automated inspection of cylindrical structures, their use could easily be extended for other types of structures.

Acknowledgment

The authors would like to thank Dr. M. Livadas, N. Lee, and Dr. N. V. Boulgouris for their comments and guidance.

References

[1] J. Rose, "Successes and challenges in ultrasonic guided waves for NDT and SHM," in *Proc. Nat. Semin. Exhib. Nondestr. Eval.*, Tiruchirappalli, India, 2009, pp. 1–18.

[2] R. E. Challis and V. Ivchenko, "Sub-threshold sampling in a correlation-based ultrasonic spectrometer," *Meas. Sci. Technol.*, vol. 22, no. 2, pp. 1–12, 2011.

[3] Z. Luo, J. Lin, L. Zeng, and F. Gao, "Mode purification for ultrasonic guided waves under pseudopulse excitation," *J. Phys. Conf. Ser.*, vol. 628, no. 1, p. 012123, 2015.

[4] L. Senni, L. Battaglini, P. Burrascano, S. Laureti, and M. Ricci, "Industrial applications: Ultrasonic inspection of large forgings," in *Ultrasonic Nondestructive Evaluation Systems*. New York, NY, USA: Springer, 2015, pp. 245–258.

[5] D. Zhang, Z. Zhou, J. Sun, E. Zhang, Y. Yang, and M. Zhao, "A magnetostrictive guided-wave nondestructive testing method with multifrequency excitation pulse signal," *IEEE Trans. Instrum. Meas.*, vol. 63, no. 12, pp. 3058–3066, Dec. 2014.

[6] Z. Zhou *et al.*, "Application of wavelet filtering and Barker-coded pulse compression hybrid method to air-coupled ultrasonic testing," *Nondestr. Test. Eval.*, vol. 29, no. 4, pp. 297–314, 2014.

[7] M. Ricci *et al.*, "Exploiting non-linear chirp and sparse deconvolution to enhance the performance of pulse-compression ultrasonic NDT," in *Proc. IEEE Int. Ultrason. Symp. (IUS)*, 2012, pp. 1489–1492.

[8] R. Sicard, J. Goyette, and D. Zellouf, "A numerical dispersion compensation technique for time recompression of Lamb wave signals," *Ultrasonics*, vol. 40, no. 1, pp. 727–732, 2002.

[9] P. Wilcox, "A rapid signal processing technique to remove the effect of dispersion from guided wave signals," *IEEE Trans. Ultrason., Ferroelectr., Freq. Control*, vol. 50, no. 4, pp. 419–427, Apr. 2003.

[10] T. Yamasaki, S. Tamai, and M. Hirao, "Optimum excitation signal for long-range inspection of steel wires by longitudinal waves," *NDT E Int.*, vol. 34, no. 3, pp. 207–212, 2001.

[11] J. Lin and L. Zeng, "Chirp-based pre-compensation for high resolution Lamb wave inspection," *NDT E Int.*, vol. 61, pp. 35–44, 2013.

[12] K. Xu, D. Ta, P. Moilanen, and W. Wang, "Mode separation of lamb waves based on dispersion compensation method," *J. Acoust. Soc. Amer.*, vol. 131, no. 4, pp. 2714–2722, 2012.

[13] K. Xu, D. Ta, B. Hu, P. Laugier, and W. Wang, "Wideband dispersion reversal of Lamb waves," *IEEE Trans. Ultrason., Ferroelectr., Freq. Control*, vol. 61, no. 6, pp. 997–1005, Jun. 2014.

[14] K. Xu, C. Liu, and D. Ta, "Ultrasonic guided waves dispersion reversal for long bone thickness evaluation: A simulation study," in *Proc. 35th Annu. Int. Conf. IEEE Eng. Med. Biol. Soc. (EMBC)*, 2013, pp. 1930–1933.

[15] K. Toiyama and T. Hayashi, "Pulse compression technique considering velocity dispersion of guided wave," *Rev. Prog. Quant. Nondestr. Eval.*, vol. 975, no. 1, pp. 587–593, 2008.

[16] L. De Marchi, A. Perelli, and A. Marzani, "A signal processing approach to exploit chirp excitation in Lamb wave defect detection and localization procedures," *Mech. Syst. Signal Process.*, vol. 39, no. 1, pp. 20–31, 2013.

[17] L. De Marchi, A. Marzani, M. Miniaci, A. Perelli, and N. Testoni, "Localization of defects in irregular waveguides by dispersion compensation and pulse compression," in *Proc. SPIE Health Monit. Struct. Biol. Syst.*, 2013, vol. 8695, pp. 965–976.

[18] K. Gröchenig, *Foundations of Time-Frequency Analysis*. New York, NY, USA: Springer, 2013.

[19] M. A. Richards, *Fundamentals of Radar Signal Processing*. New York, NY, USA: McGraw-Hill, 2005.

[20] D. Hutchins, P. Burrascano, L. Davis, S. Laureti, and M. Ricci, "Coded waveforms for optimised air-coupled ultrasonic nondestructive evaluation," *Ultrasonics*, vol. 54, no. 7, pp. 1745–1759, 2014.

[21] M. Ricci, L. Senni, and P. Burrascano, "Exploiting pseudorandom sequences to enhance noise immunity for air-coupled ultrasonic nondestructive testing," *IEEE Trans. Instrum. Meas.*, vol. 61, no. 11, pp. 2905–2915, Nov. 2012.

[22] E. Pardo, J. L. San Emeterio, M. A. Rodriguez, and A. Ramos, "Noise reduction in ultrasonic NDT using undecimated wavelet transforms," *Ultrasonics*, vol. 44, pp. 1063–1067, 2006.

[23] M. K. Yucel *et al.*, "Pulse-compression based iterative time-of-flight extraction of dispersed ultrasonic guided waves," in *Proc. 13th IEEE Int. Conf. Ind. Inf. (INDIN)*, 2015, pp. 809–815.

[24] B. Engineer, "The mechanical and resonant behaviour of a dry coupled thickness-shear PZT transducer used for guided wave testing in pipe line," Ph.D. dissertation, School Eng. Design, Brunel Univ., Middlesex, U.K., 2013.

[25] M. Legg, M. K. Yücel, V. Kappatos, C. Selcuk, and T.-H. Gan, "Increased range of ultrasonic guided wave testing of overhead transmission line cables using dispersion compensation," *Ultrasonics*, vol. 62, pp. 35–45, 2015.

Mehmet Kerim Yücel received the B.Sc. degree in electrical and electronics engineering from Bilkent University, Ankara, Turkey, in 2011, and the M.Sc. degree (with distinction) in wireless communication systems and the M.Phil. degree with an emphasis on signal processing and machine learning applied to defect detection in complex structures from Brunel University, Uxbridge, U.K., in 2012 and 2015, respectively.

He was a Teaching Assistant with the University of Pompeu Fabra, Barcelona, Spain. Currently, he is working as an Embedded Software Engineer with Meteksan Defense Industry Inc., Ankara. Throughout his career, he has worked on various EU and U.K. government funded projects, military projects funded by the Turkish Armed Forces. He has authored several high-profile journal and conference papers. His research interests include statistical signal processing, machine learning, ultrasonics, computer vision, and telecommunications.

Sina Fateri was born in Babol, Iran. He received the B.Sc. (Hons.) degree in computer science from the University of Mazandaran, Babolsar, Iran, in 2009, and the M.Sc. (Hons.) degree in wireless communications engineering from Brunel University, Uxbridge, U.K., in 2011, where he is currently pursuing the Ph.D. degree in electronic systems research based at TWI Ltd., Cambridge, U.K.

He was a Graduate Teaching Assistant with the Wireless Communications Laboratory, TWI Ltd., from 2011 to 2013. Since 2015, he has been a Project Leader (Technology) with Plant Integrity Ltd., Cambridge, where he is performing signal processing for industrial sectors. His research interests include advanced signal processing techniques for ultrasonic guided wave inspections, acoustic signal processing, mode identifications in ultrasonic guided wave inspections, ultrasonic guided wave mode conversion from discontinuities, and long-term monitoring of large complex structures.

Mathew Legg received the B.Sc., M.Sc., and Ph.D. degrees in physics from the University of Auckland, Auckland, New Zealand, in 2003, 2007, and 2012, respectively.

Subsequently, he was a Research Fellow with the University of Auckland, where he lectured on signal processing and performed research on acoustic imaging of defects in wood. In 2013, he joined the Brunel Innovation Centre, Uxbridge, U.K., where he was a Project Leader on several EU projects on ultrasonic guided wave nondestructive testing. Currently, he is a Postdoctoral Fellow with the University of Auckland, where he is developing acoustic/ultrasonic nondestructive testing tools for measuring the structural properties of tree stems.

Adam Wilkinson received the Ph.D. degree in magnetic resonance imaging from the University of Cambridge, Cambridge, U.K.

He has a background in electronics, software, and systems engineering. He has been working in nondestructive testing at TWI Ltd., Cambridge, U.K., for four years, and is now working for a wholly owned subsidiary of TWI, Plant Integrity Ltd.

Vassilios Kappatos received the Ph.D. degree in nondestructive testing from the Department of Electrical and Computer Engineering, University of Patras, Patras, Greece, in 2007, and the M.Eng. degree in mechanical and aeronautical engineering from the University of Patras, in 2002.

He has been a Key Researcher on many funded research projects. He has authored over 80 publications in international journals, conference proceedings, and book chapters. He is also a Referee of several international journals and conferences. Throughout his career, he has lectured a broad range of subjects in the area of applied engineering both in U.K. and Greece. His research interests include structural integrity, nondestructive testing, structural health monitoring, signal processing, pattern recognition, and material behavior.

Cem Selcuk received the Ph.D. degree from the Department of Mechanical, Materials, and Manufacturing Engineering, University of Nottingham, Nottingham, U.K., in 2003.

Currently, he is the Manager and Head of the Brunel Innovation Centre, Uxbridge, U.K., established in 2009 jointly with Brunel University, Uxbridge, and TWI Ltd., Cambridge, U.K. Following the Ph.D. degree and after taking part in a multinational EU project as a Research Associate, he moved into industry as a Project Manager in Product and Technology Development. He has authored over 120 citations to his publications (over 50) in peer-reviewed journals, international conferences, book chapters, and industrial project reports. His research interests include development of alternative materials processing techniques and technology transfer, with an emphasis on the relationship between processing, structure, and properties of materials for improved performance and quality control; materials design in the field of powder metallurgy and metal matrix composites; and advanced nondestructive evaluation methods and their automation for a wide range of applications.

Tat-Hean Gan received the B.Sc. degree in electrical and electronics engineering (first class Hons.) from the University of Nottingham, Nottingham, U.K.; the M.Sc. (with distinction) and Ph.D. degree in mechanical engineering and ultrasonic imaging from the University of Warwick, Coventry, U.K., in 2002; and the EMBA degree from the University of Birmingham, Birmingham, U.K.

Currently, he is a Professor with Brunel University, Uxbridge, U.K., where he is the Chair of Acoustic Waves Technologies in the School of Engineering and Design. He is an Associate Director at TWI Ltd., Cambridge, U.K., and Technology Director of the National Structural Integrity Research Centre (NSIRC). He has authored over 100 papers and has contributed to several books in Non-Destructive Testing (NDT) field. His research interests span signal and image processing, sensor development, and asset integrity.

Dr. Gan has obtained the Chartered Engineer, European Engineer, International Professional Engineer (U.K.) Status, and has been a Fellow of the Institute of Engineering and Technology and the British Institute of Non-Destructive Testing since 2011.